

'Cleanroom' in SEM

Jeevanandam, G.; van der Meijden, V.; Birnie, L. D.; Kruit, P.; Hagen, C. W.

DOI

[10.1016/j.mee.2020.111239](https://doi.org/10.1016/j.mee.2020.111239)

Publication date

2020

Document Version

Final published version

Published in

Microelectronic Engineering

Citation (APA)

Jeevanandam, G., van der Meijden, V., Birnie, L. D., Kruit, P., & Hagen, C. W. (2020). 'Cleanroom' in SEM. *Microelectronic Engineering*, 224, Article 111239. <https://doi.org/10.1016/j.mee.2020.111239>

Important note

To cite this publication, please use the final published version (if applicable). Please check the document version above.

Copyright

Other than for strictly personal use, it is not permitted to download, forward or distribute the text or part of it, without the consent of the author(s) and/or copyright holder(s), unless the work is under an open content license such as Creative Commons.

Takedown policy

Please contact us and provide details if you believe this document breaches copyrights. We will remove access to the work immediately and investigate your claim.

Green Open Access added to TU Delft Institutional Repository

'You share, we take care!' - Taverne project

<https://www.openaccess.nl/en/you-share-we-take-care>

Otherwise as indicated in the copyright section: the publisher is the copyright holder of this work and the author uses the Dutch legislation to make this work public.



ELSEVIER

Contents lists available at ScienceDirect

Microelectronic Engineering

journal homepage: www.elsevier.com/locate/mee

Research paper

‘Cleanroom’ in SEM

G. Jeevanandam*, V. van der Meijden, L.D. Birnie, P. Kruit, C.W. Hagen

Delft University of Technology, Dept. Imaging Physics, Lorentzweg 1, 2628CJ Delft, the Netherlands

ARTICLE INFO

Keywords:

SEM
Nanofabrication
Sputter etching
Thermal evaporation

ABSTRACT

To allow researchers to fabricate micro- and nano-devices on a small scale, without having to use complex cleanroom facilities, a single tool is proposed in which a variety of typical cleanroom techniques and processes is combined. This ‘cleanroom’ in SEM tool, based on a scanning electron microscope (SEM), integrates several add-on tools, such as a miniature plasma source for sputtering and cleaning purposes, a miniature thermal evaporator for metal deposition, and facilities to enable in-situ selective atomic layer deposition. The cleanroom techniques and processes selected for integration in the ‘cleanroom’ in SEM tool are discussed, and the design and fabrication of the add-on tools are presented. Finally the proofs of principle of the plasma source, evaporator and in-situ selective ALD process are experimentally demonstrated.

1. Introduction

Micro- and nanoscale devices are routinely fabricated in dedicated cleanrooms to avoid defects due to particles and contamination. The equipment available in cleanrooms is usually designed for wafer scale processing, ranging from 4 to 12-inch wafers. However, many researchers in academia do not need full wafers with devices, but often only need a few devices. The total device area is probably a few μm^2 only, and the substrates that are mounted in scientific measurement setups are of the order of 1 cm^2 in size. In this work we describe a dedicated instrument for the fabrication of such small-scale devices, avoiding entirely the need for a conventional cleanroom facility. The instrument is based on a dual beam instrument, a combination of a scanning electron microscope (SEM) and a focused ion beam (FIB) system. It is a vacuum system, and therefore free of dust particles, it offers electron-beam inspection as well as electron-beam patterning, provided it is equipped with a pattern generator. Adding gas injection systems (GIS) also allows for focused electron (ion) beam induced processing (FE(I)BIP) to deposit or remove materials [1]. Compositional analysis by energy dispersive X-ray spectroscopy (EDX or EDS) is possible by adding an X-ray detector. A system with all these components is already commercially available for a fraction of the cost of a full-fledged cleanroom facility. However, to be able to fabricate devices in such a system, without the need to take them out of the system in between process steps, requires more process add-on's. In the next section a typical cleanroom process flow is considered, to aid in selecting the additional processes that can be integrated in the ‘cleanroom’ in SEM tool. The system is coined ‘cleanroom’ in SEM because the functionality

of all tools put together in an SEM resembles that of a dedicated cleanroom facility.

2. Selection of add-on processes for ‘cleanroom’ in SEM

The SEM environment clearly imposes restrictions on the tools and materials to be added. First of all there are vacuum requirements. An SEM operates at a chamber pressure of 10^{-6} to $9 \cdot 10^{-5}$ mbar. Whereas the chamber pressure is in the high vacuum range, the electron gun is kept at ultra-high vacuum (10^{-9} to 10^{-10} mbar). The gun area and the vacuum chamber are separated by differential pumping. An increase of the chamber pressure beyond $9 \cdot 10^{-5}$ mbar will trigger closing of the valve between the gun area and the optical column and specimen chamber. Any material brought inside the SEM chamber should not outgas, as it will lead to a pressure increase and it may contaminate the specimen chamber. Any contamination in the chamber can travel to the aperture where it can be deposited, leading to charging, thereby affecting the beam quality. In addition, contamination will lead to deposition on the substrate whenever it is exposed to the electron beam. This is typically observed as the darkening of the SEM image after parking or scanning the beam. To prevent contamination of the chamber and its added components, each element brought into the SEM should be thoroughly cleaned in acetone followed by ethanol or isopropanol.

Also the beam quality poses requirements on the materials added to the SEM. Insulating materials in direct line of sight of a charged particle beam will result in charging, and subsequent beam deflection or distortion. Similar effects will be caused by spurious magnetic fields in the

* Corresponding author.

E-mail address: g.jeevanandam@tudelft.nl (G. Jeevanandam).<https://doi.org/10.1016/j.mee.2020.111239>

Received 18 November 2019; Received in revised form 19 January 2020; Accepted 3 February 2020

Available online 04 February 2020

0167-9317/ © 2020 Elsevier B.V. All rights reserved.

Table 1
Process parameters of different fabrication tools.

Cleanroom techniques	Operating conditions				SEM compatibility		
	Operating pressure (mbar)	Temperature (°C)	Gases used	Control units	Pressure	Temperature	Material
Wet clean	1000	RT to 70	Liquid chemical	Hot plate	X	X	X
Dry Clean	0.1 to 10	300–800	O ₂ , Ozone	RF, UV light	✓	X	✓ ^a
Oxidation	1000	700–1200	O ₂ , H ₂ O	heater	X	X	✓ ^a
Local oxidation	10 ⁻⁵	RT	H ₂ O, O ₂	e-beam	✓	✓	✓ ^a
Evaporation	10 ⁻⁶ to 10 ⁻⁸	RT	None	Resistive or e-beam	✓	✓	✓ ^a
Sputter deposition	10 ⁻¹ to 10 ⁻²	RT	Ar	RF or DC	X	X	✓ ^a
LPCVD	1 to 10 ⁻¹	700–1100	N ₂ , precursor	furnace	X	X	✓ ^a
PECVD	10 ⁻²	100–400	Ar, CH ₄ , SiH ₄	RF or microwave	X	X	✓ ^a
ALD	1 to 25	100–300	Precursor and co-reactant	RF, substrate heater	X	X	✓ ^a
Resist coating	1000	50–200	Resist	Spinner	X	X	X
E-beam lithography	10 ⁻⁶	RT	None	e-beam	✓	✓	✓
Sputter etching	1 to 10 ⁻³	RT	Ar	DC, RF	X	✓	✓ ^a
Plasma etching	0.1 to 1	RT	O ₂ , Cl ₂	RF	X	✓	✓ ^a
RIE	0.1 to 10	- 150 - 30	BCl ₃ , Cl ₂ , SF ₆ , CHF ₃ , Ar	RF	X	X	✓ ^a
Resist stripping	1	150–300	O ₂	RF	X	X	✓ ^a
Inspection							
EDX	10 ⁻⁶ to 10 ⁻⁵	RT	None	e-beam	✓	✓	✓
SEM	10 ⁻⁵ to 10 ⁻⁶	RT	None	e-beam	✓	✓	✓
AFM	1000 to 10 ⁻⁶	RT	None	AFM unit	✓	✓	✓
FIB	10 ⁻⁶ to 10 ⁻⁵	RT	None	I-beam	✓	✓	✓

RT – room temperature, LPCVD – low pressure chemical vapour deposition, PECVD- plasma enhanced CVD, ALD – atomic layer deposition, RIE – reactive ion etching, RF- radio frequency, DC- direct current, UV – ultra violet, EDX- energy dispersive X-ray spectroscopy, AFM- atomic force microscopy, FIB – focussed ion beam.

^a Modified GIS for gas delivery.

chamber, therefore all components inside the SEM should be made of non-magnetic materials.

A typical cleanroom process flow for the fabrication of a device may contain the following steps: cleaning, deposition, lithography (spin coating of resist, exposure and development), etching, resist stripping and inspection. Table 1 lists the various cleanroom processes and tools, that can be involved in such a process flow, together with their operating conditions. The table also indicates whether the operating temperatures and pressures, and materials used, are compatible with the SEM environment.

The first step in any process flow is substrate cleaning. Wet chemical-based cleaning is not really compatible with an SEM, but dry-cleaning is. SEM's are often equipped with a commercial plasma cleaner to clean the specimen and specimen chamber. The application of resist in SEM will be difficult too, but patterning can also be achieved by using masks fabricated by FEBIP [2,3]. Any pattern can be deposited, using this technique, on a pre-deposited device layer, and subsequently transferred into the device layer using a plasma etching process. Because FEBIP-fabricated deposits often contain carbon-containing fragments, originating from the precursor molecules used, they are well suited as etching masks, but less well suited to function as device layers [4,5]. Therefore, an additional deposition tool is desired, for the deposition of pure materials, and a plasma tool for pattern transfer. The latter could also be used for substrate cleaning, and possibly for local oxidation as well.

To select a deposition tool there are several possibilities. For physical vapour deposition (PVD) one can choose between sputter deposition and thermal evaporation. Both require vacuum, but sputter deposition requires a glow discharge at pressures too high for operation in an SEM, and the deposition is not very directional, causing the risk of unwanted deposition on dielectrics. Thermal evaporation is much more compatible with the SEM conditions. The substrate is typically kept at room temperature, the deposition is directional and, when the distance to the substrate is kept small, the area of deposition is also limited. Therefore, it is feasible to integrate a thermal evaporation source into an SEM, the design of which will be discussed in the next section.

For chemical vapour deposition (CVD) one can choose among low-pressure CVD (LPCVD), plasma-enhanced CVD (PECVD) and atomic layer deposition (ALD). LPCVD can be eliminated, as it operates at

pressures too high for normal SEM operation, and it requires substrate temperatures above 600 °C. PECVD requires a plasma, operates at even higher pressures and requires substrate temperatures of 300 °C. This process can be eliminated too. In commercial reactors ALD operates at high pressure with substrate temperatures around 300 °C. At first glance, this technique also conflicts with the SEM. But, as in FEBIP, one can use a GIS that creates locally a high pressure at the surface of the substrate. In addition, both Pt FEBIP and Pt ALD make use of the same precursor, MeCpPtMe₃ [6]. Area selective ALD, using Pt FEBIP as a seed layer, is a direct write technique which combines the high resolution of FEBIP with the high purity of ALD [7,8]. Requirements for implementing this technique are that O₂ gas needs to be injected as a co-reactant and the substrate needs to be heated to 300 °C. As already demonstrated by [9], and as will be seen in the next sections, it is feasible, utilizing the GIS to deliver the required gas pressure locally near the substrate, to integrate area selective ALD in an SEM.

An important step in the process flow is etching. Here the choices are reactive ion etching (RIE), plasma etching and sputter etching. RIE operates at pressures of 10 to 10⁻¹ mbar, substrate temperatures of 150 to 300 °C and a plasma to create the reactive ions. It requires the use of reactive gases such as SF₆, SiCl₄, etc., which may attack the objective lens pole piece, the specimen stage or the electron and X-ray detectors. So, RIE can be eliminated. Plasma etching operates at pressures of 0.1 to 1 mbar, and also requires a plasma and the use of reactive gases. Hence, we can eliminate this too. This leaves the most basic type of etching tool: sputter etching. It operates at 1 to 10⁻³ mbar pressure, and requires a plasma for the generation of ions. The main challenge to make this work in the SEM is to bridge the gap in pressure between the SEM vacuum and the plasma pressure. We will show in the next section that this is possible indeed.

For inspection the SEM already provides high resolution imaging, and, in combination with the FIB, also cross-sectional analysis, but for accurate step height measurements atomic force microscopy (AFM) is desired as well, and can be integrated in an SEM as well [10].

The addition to an SEM, of a miniature sputter etching tool and a miniature thermal evaporation tool, for local deposition, enables the fabrication of an entire device, such as e.g. a bow tie antenna, in the SEM, without breaking the vacuum between different process steps. To just give an example of the typical process flow for the fabrication of a

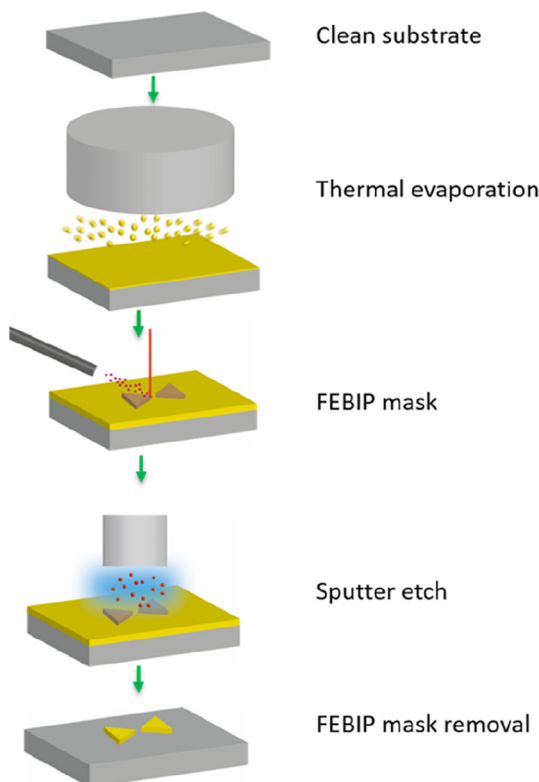


Fig. 1. Proposed process flow for the in-SEM fabrication of a bow tie antenna, using the SEM add-on tools discussed in the text.

bow tie antenna a schematic overview of the process is shown in Fig. 1. It begins with loading a clean substrate into the SEM. A layer of the antenna material (e.g. gold) is locally deposited using the miniature thermal evaporator. Then a FEBIP-fabricated mask (for instance carbon) is patterned on top of the antenna material layer, to serve as a hard mask in the subsequent pattern transfer step. The latter is done using the miniature sputter etching tool. Finally, we remove the remaining FEBIP mask using electron beam-induced etching (H_2O), leaving the desired bow tie antenna on the substrate [11].

3. Design of the miniature add-on tools

An important requirement for the plasma source is that it should operate within the operating parameters of the SEM. When in operation the chamber pressure should typically be of the order of 10^{-5} mbar. Any increase in chamber pressure beyond $9.9 \cdot 10^{-5}$ mbar will result in the venting of the SEM. All materials used should be non-magnetic, vacuum compatible with low outgassing rates, and insulating materials have to be shielded from the charged particle beam. Furthermore, the plasma source needs to be miniaturized as the space available in the SEM is limited. Preferably the plasma source can be used underneath the optical column, while operating the electron beam. This, for instance, would allow SEM imaging to monitor the sputtering process or to serve as an end stop. And, when using an oxygen plasma, placing the source under the column could be useful to remove contamination during imaging, or to remove carbon from FEBIP deposits. Such applications would favour a DC operated source over an AC operated one, to avoid disturbances to the electron beam. Therefore a DC source was developed, but, to demonstrate the feasibility of running a plasma source in an SEM to achieve sputtering at the vacuum levels of the SEM, initially a less challenging mechanical design was chosen of a plasma source not mounted directly under the column, but at some distance from the objective lens.

A schematic drawing of the plasma source is shown in Fig. 2. A piece

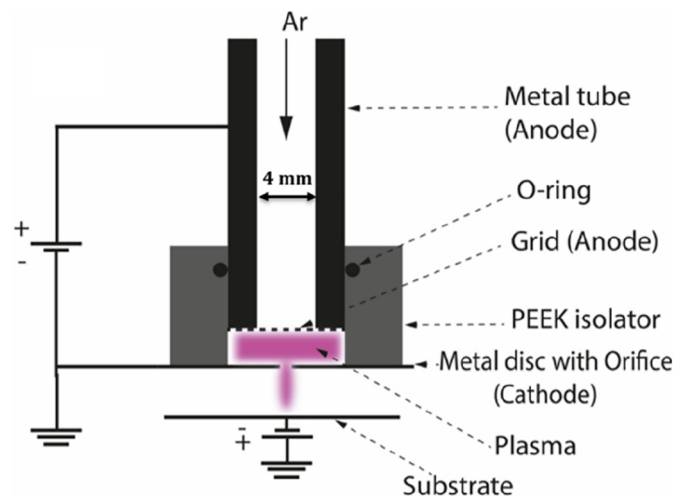


Fig. 2. Schematic drawing of the miniature plasma source.

of standard $\frac{1}{4}$ "Swagelok tubing was used as the anode and also serves as the gas supply. Argon was used as a gas in this study. An electrically insulating PEEK cylinder was fitted around the Swagelok tube extending slightly beyond its end. A tungsten grid is placed inside the PEEK cylinder, making electrical contact to the Swagelok tubing, i.e. the anode. The cathode consists of a plate of phosphor bronze with an orifice of $50 \mu\text{m}$ in diameter, and is glued to the end of the PEEK insulator using vacuum compatible double sided Kapton tape from Accu-Glass products. The distance between the tungsten grid and the orifice plate is $500 \mu\text{m}$. The orifice is chosen sufficiently small to maintain a pressure inside the plasma chamber large enough to sustain the plasma, while the pressure outside of the plasma chamber is around 10^{-5} mbar.

The evaporation source has to fulfil similar requirements as the plasma source. To miniaturize the thermal evaporation source a Philips I cathode source was used, originally applied in cathode ray tube (CRT) monitors. The source is a thermionic electron source which operates by resistively heating a cathode until it emits electrons. The voltage across the heater filament controls the temperature of the cathode. The original source has been adapted such that a small cylindrical container, made from Molybdenum, fits tightly over the cathode. This container holds the material to be evaporated and is capped with a closely fitting lid, also made from Molybdenum with an 0.2 mm diameter (d_a) central orifice. A schematic drawing of the cathode with the assembly to hold the material is shown in Fig. 3. An outer cylinder made from stainless steel which acts as a heat shield, with a central orifice of 0.5 mm diameter (d_b), is placed over the body of the cathode source. In this study gold was chosen as the material to be deposited. To this end the inner cylinder was filled with Au foil. It was carefully checked that the cathode itself does not evaporate leading to unwanted deposition.

To implement ALD in the SEM, co-reactant gas has to be delivered to the substrate. This was achieved by modifying the needle of an existing gas injection system (GIS) such that gas from outside, fed in through a gas feedthrough, enters the needle. Dry air was chosen as the co-reactant gas in this study. To heat the substrate a heater was developed with a maximum temperature of $250 \text{ }^\circ\text{C}$. It was designed mechanically such the centre has minimum drift due to thermal expansion. It was designed, and also tested, such that the temperature of the stage was at room temperature even when the substrate is kept at $250 \text{ }^\circ\text{C}$. It can accept samples of $1 \times 1 \text{ cm}^2$ size.

To demonstrate the proof of principle of the add-on tools and not endanger the performance of the SEM, experiments were performed in a separate vacuum system. The system is built using ultra-high-vacuum (UHV) components, although for these experiments it is not used at UHV pressures. The system is pumped with a turbo-molecular pump and a scroll pump as a pre-vacuum pump. The chamber pressure is

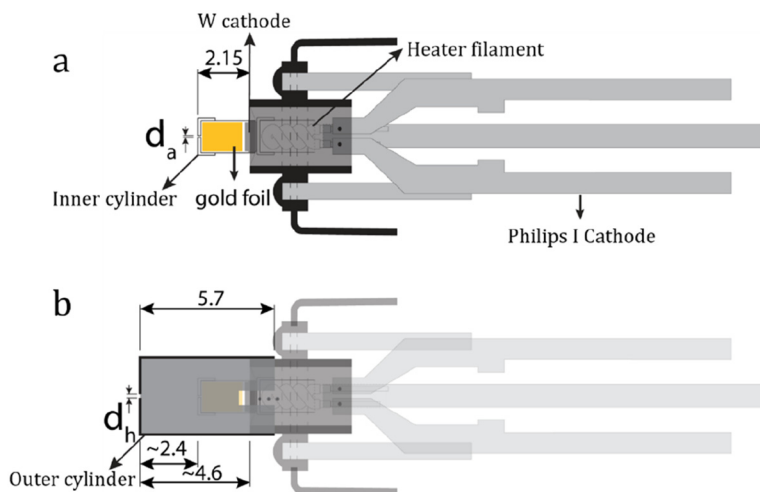


Fig. 3. a) Sketch of the thermal evaporation source showing the Philips I cathode with the W cathode, heater filament and the inner cylinder with an orifice diameter (d_a) of 0.2 mm. b) Sketch of the thermal evaporation source with the outer cylinder, with an of 0.5 mm diameter orifice (d_h), placed over the cathode body. All dimensions indicated are in mm.

measured by a Bayard-Alpert hot cathode gauge. Both the plasma source and the thermal evaporator assembly are mounted onto an adapter and suspended above the substrate. The adapter is attached to a four degrees of freedom manipulator (x, y, z and one rotation around the suspension axis). This allows proper positioning of both the plasma source and the evaporator above the substrate. Argon gas is delivered to the plasma source through a gas feedthrough. The gas pressure supplied to the plasma source is controlled by a Bronkhorst EL-PRESS pressure controller. The high voltage supply (Fug power supply MCN 14–2000) is connected to the electrodes through electrical feedthroughs. The substrate is kept at a raised potential by means of a series of DC batteries with a maximum voltage of 250 V. The potential drop across the electrodes is measured by two digital multimeters. The plasma current between the electrodes and the current at the substrate are measured using a Keithley 6485 pico-ammeter. The power for the thermal evaporation source is delivered through electrical feedthroughs from a Delta Elektronika ES 030–5 power supply.

The ALD setup was tested in a Nova Nano Lab 600i dual beam instrument from Thermo Fisher scientific, using MeCpPtMe₃ as a precursor gas introduced from one GIS needle, and dry air introduced from another modified GIS needle and using a custom built in-situ substrate heater (see Fig. 4).

A Dektak XT profiler was used to measure the height profile of the deposit from the miniature thermal evaporation tool. An AFM-in-SEM instrument from nano analytic GmbH [10] was used to measure layer thickness after the in-situ ALD experiments.

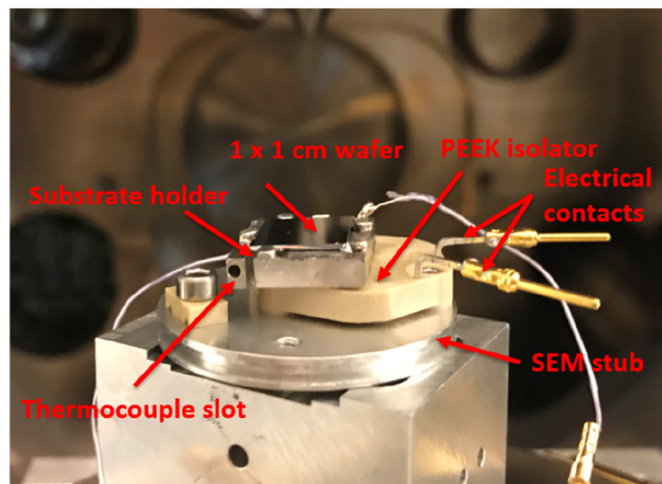


Fig. 4. Photograph of the in-situ substrate heater mounted on the SEM stage.

4. Results and discussion

First it was tested whether the plasma source can sustain a plasma while the pressure outside of the source is at SEM operating pressure. Initially the Ar inlet pressure, i.e. the pressure in the plasma chamber between the two electrodes, was kept at 30 mbar, while increasing the voltage between the electrodes until a current between the electrodes is observed. A plasma current of 5 μ A was observed at the breakdown voltage. A photograph of the observed plasma is shown in the inset of Fig. 5 (the blue dot in the centre). Subsequently the Paschen curve (breakdown voltage versus product $p \cdot d$ of pressure p and electrode distance d) was measured by varying the inlet pressure from 2 to 200 mbar and recording at which voltage breakdown is observed. The data are shown in Fig. 5. From the graph can be determined at which pressure the plasma operates at minimum voltage. Preferably the source is operated at the lowest possible voltage to keep voltages inside the SEM chamber at a low value to avoid flash-overs. While recording the Paschen curve the pressure outside of the plasma source was registered. It varied from $9 \cdot 10^{-6}$ mbar to $1 \cdot 10^{-3}$ mbar. The chamber pressure remained within the limits of the SEM operating pressure

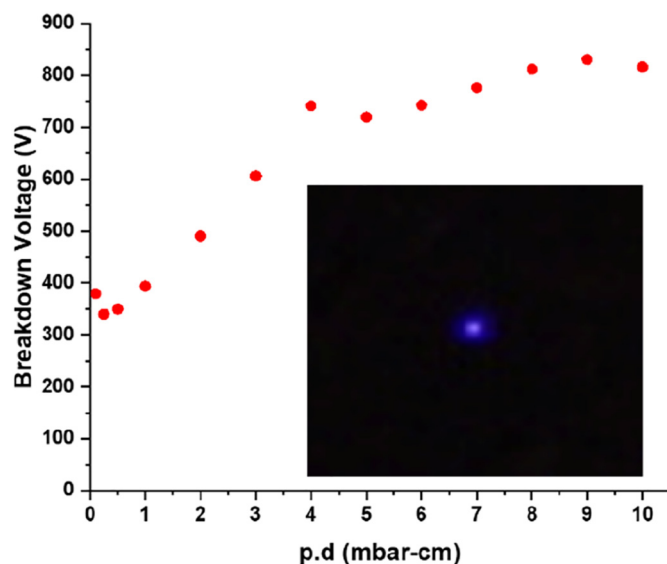


Fig. 5. Graph showing the measured Paschen curve with a constant electrode spacing of 0.5 mm. The inset shows a photograph of the plasma observed through the orifice (the blue dot in the centre of the image). (For interpretation of the references to colour in this figure legend, the reader is referred to the web version of this article.)

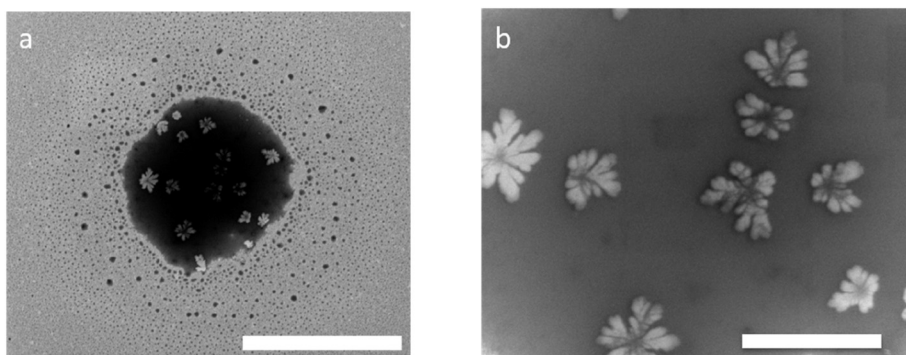


Fig. 6. a) Secondary electron image of an area etched into a 200 nm thick Au film using the miniature plasma source, scale bar is 20 μm . b) Secondary electron image of the etched pit showing some remaining gold structures on the silicon substrate, proving that most of the gold film has been removed, scale bar is 5 μm . (For interpretation of the references to colour in this figure legend, the reader is referred to the web version of this article.)

(< 10^{-5} mbar) while operating the source at an inlet pressure between 2 and 15 mbar. To test the plasma source as a miniature sputter tool, it was operated at an inlet pressure of 5 mbar. A silicon substrate was coated with a 200 nm thick Au film. The Au-coated Si substrate was kept at a distance of 0.5 mm from the plasma source and exposed to the plasma for 30 min while keeping the substrate at -250 V. The plasma current between the electrodes was 50 μA , and the substrate current was 0.43 nA. After 30 min of plasma exposure, the substrate was taken out of the vacuum setup and inspected in an SEM. The secondary electron image of the etched area is shown in Fig. 6. Local etching of the Au film is observed over a circular area of about 20 μm in diameter. With a measured substrate current of 0.43 nA, and assuming that this is the Ar ion current, and a sputter yield of 1 atoms/ion at an ion energy of 250 V [12], the etching rate is calculated to be 1.4 $\text{\AA}/\text{s}$. To completely etch a 200 nm thick Au film would then take 24 min, in good agreement with the observed 30 min to remove the gold film. Fig. 6b shows some remaining gold structures on the silicon substrate, proving that most of the gold film has been removed. The further characterization of the miniature sputter tool will be the subject of a forthcoming separate publication.

The miniature thermal evaporation source was tested by locally depositing a gold film onto a silicon substrate. The distance between the outer shield of the thermal evaporation source and the Si wafer was kept at a distance of 2 mm, and 14 V was supplied across the heater filament. After 5 min of deposition the voltage was slowly reduced to zero. The Si wafer was inspected under an optical microscope and a local gold coloured circular deposit is observed, about 0.8 mm in diameter (see Fig. 7). The thickness of the deposit was measured as 140 nm

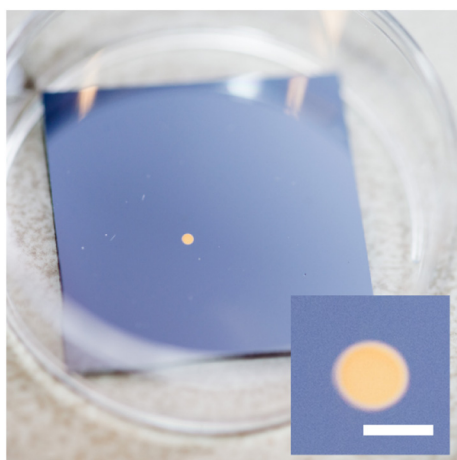


Fig. 7. Photograph of a $23 \times 23 \text{ mm}^2$ silicon sample with a gold disc locally deposited from the miniature thermal evaporation tool. The inset is a zoomed-in image of the deposited gold, with a scale bar of 1 mm. (For interpretation of the references to colour in this figure legend, the reader is referred to the web version of this article.)

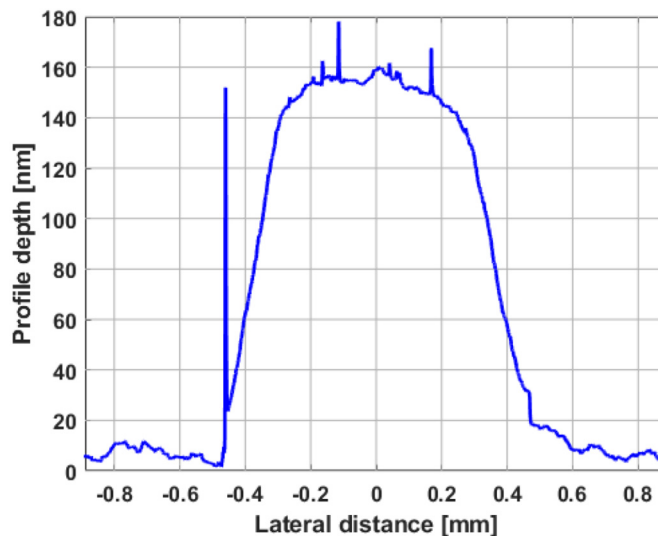


Fig. 8. Graph showing the height profile of the deposited gold. (For interpretation of the references to colour in this figure legend, the reader is referred to the web version of this article.)

using a profilometer, and the height profile is shown in Fig. 8. The detailed characterization of the miniature evaporation tool will be explained in a future publication as well.

Finally, in addition to the tools mentioned in the proposed workflow an in-situ ALD in the SEM was demonstrated. As a first step a clean Si substrate was patterned with Pt/C seed layers, using FEBIP, at a dose of 0.001, 0.01, 0.02, 0.04, 0.05, 0.06, 0.08, 0.1, 0.2 and 1 $\text{nC}/\mu\text{m}^2$. The patterns were repeated on a control wafer to determine the growth after the ALD process. The secondary electron image of the Pt/C seed layers is shown in Fig. 9a. The ALD process was started once a base pressure of $4 \cdot 10^{-6}$ mbar was reached, to minimize the effect of background water vapour and other contaminants present in the SEM chamber. Subsequently the temperature of the substrate is ramped up to 241 $^\circ\text{C}$ and the substrate is baked in a dry air environment (chamber pressure of $2.5 \cdot 10^{-5}$ mbar) to purify (i.e. reduce the carbon content of) the deposited seed layers. Fig. 9b shows the AFM profile over a seed layer after purification, the thickness of which is about 0.3 nm. After the purification step, 17 cycles of ALD are done according to the following recipe: dose the Pt-precursor for 15 s, pump for 120 s, dose the dry air for 15 s and pump for 30 s. After the ALD cycles, a clear contrast change is observed in the secondary electron image of the deposited layers (see Fig. 9c). From AFM measurement the thickness increase due to the ALD process was determined as 0.7 nm (Fig. 9d), in agreement with literature values for Pt ALD growth at 250 $^\circ\text{C}$ [13]. This agreement is remarkable because the pressures used in the in-situ ALD process described here are much lower than in [14]. Although this demonstrated in-situ area selective ALD in the SEM, a single ALD cycle takes 3 min.

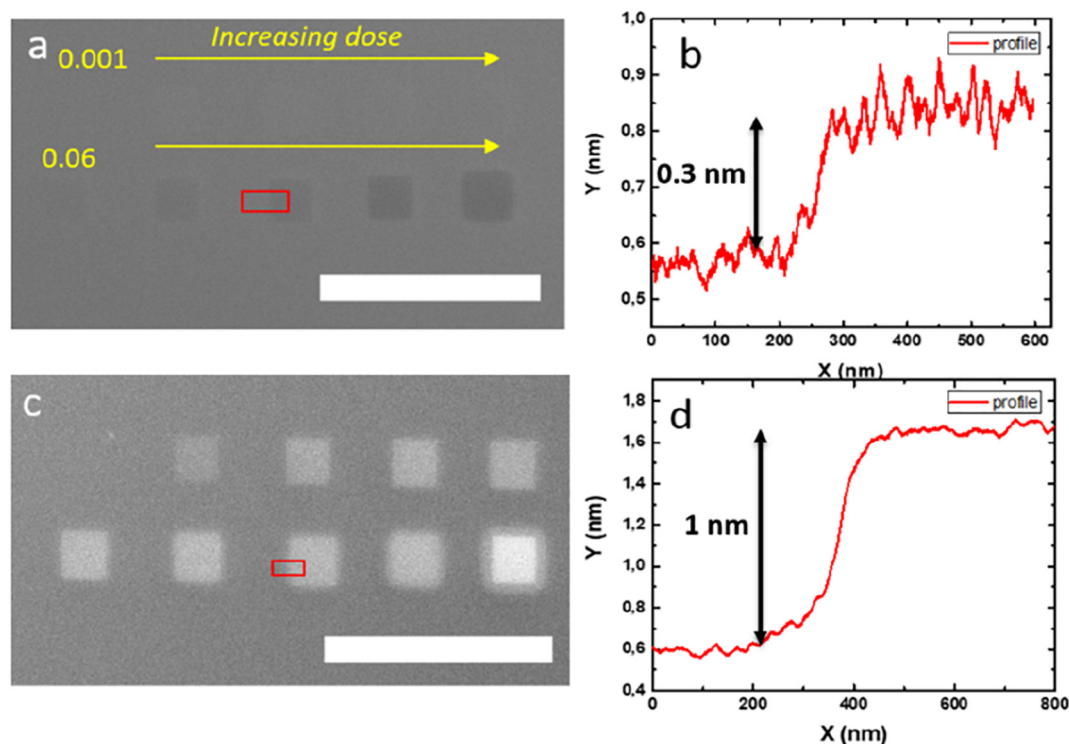


Fig. 9. a) Secondary electron image (contrast enhanced) of the Platinum seed layers deposited using FEBIP at various doses (indicated in $\text{nC}/\mu\text{m}^2$). The layers in the upper row are so thin that they can hardly be seen in the image. b) AFM profile over the seed layer indicated by the red box in a). c) Secondary electron image of the same seed layers after 17 cycles of ALD, with a clearly observed contrast change. d) AFM profile of the deposited layer indicated by the red box in c) after 17 cycles of ALD. The scale bar is $5\ \mu\text{m}$. (For interpretation of the references to colour in this figure legend, the reader is referred to the web version of this article.)

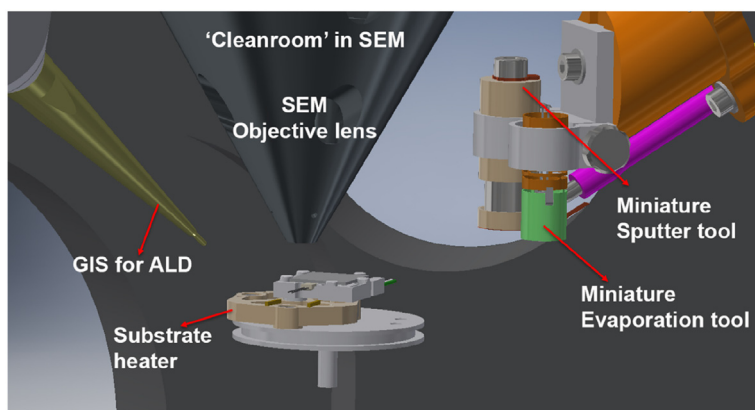


Fig. 10. CAD illustration of the 'Cleanroom' in SEM add-ons integrated in a scanning electron microscope.

Clearly the cycle time needs to be shortened to be comparable with commercial ALD tools. How this can be achieved will be discussed in a separate publication. The CAD illustration in Fig. 10 and the actual photograph in Fig. 11 show an overview of the miniature tools as integrated in the SEM. In this first prototype 'cleanroom' in SEM the plasma source and miniature evaporator are placed at some distance from the optical column.

5. Conclusions

An affordable single instrument is proposed that combines a variety of techniques and processes, which are usually only available in expensive cleanroom facilities, to fabricate small numbers of devices on small scale substrates. As the instrument is based on a scanning electron microscope (SEM) the instrument is coined 'cleanroom' in SEM. Add-on tools, such as a miniature sputter tool and a miniature thermal

evaporator were designed, built and demonstrated. A gold film was successfully deposited locally using the thermal evaporation tool, and also successfully removed locally using the miniature sputter tool. Furthermore, a dedicated heater and a modified gas injection system allowed to perform in-situ area selective ALD in this instrument. This was demonstrated using seed layers deposited with FEBIP followed by ALD cycles using MeCpPtMe_3 as a precursor gas. The 'cleanroom' in SEM is also equipped with a FIB, EDX, AFM and several gas injection systems. A versatile system is obtained that may well serve scientists in academia to fabricate single prototype devices, involving many process steps, and no need to take the device out of the vacuum chamber between process steps.

Declaration of Competing Interest

The authors declare that they have no known competing financial

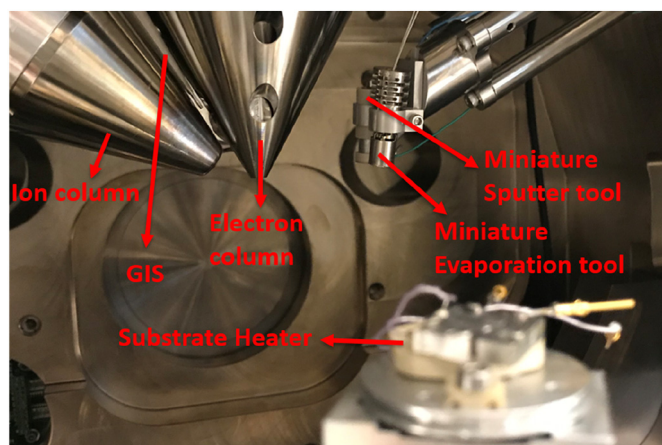


Fig. 11. Photograph of the actual 'Cleanroom' in SEM add-ons integrated in a scanning electron microscope.

interests or personal relationships that could have appeared to influence the work reported in this paper.

Acknowledgments

This research did not receive any specific grant from funding agencies in the public, commercial, or not-for-profit sectors.

References

- [1] I. Utke, P. Hoffmann, J. Melngailis, Gas-assisted focused electron beam and ion beam processing and fabrication, *J. Vac. Sci. Technol. B.* 26 (2008) 1197, <https://doi.org/10.1116/1.2955728>.
- [2] C.T.H. Heerkens, M.J. Kamerbeek, W.F. van Dorp, C.W. Hagen, J. Hoekstra, Electron beam induced deposited etch masks, *Microelectron. Eng.* 86 (2009) 961–964, <https://doi.org/10.1016/j.mee.2008.11.079>.
- [3] I.G.C. Weppelman, P.C. Post, C.T.H. Heerkens, C.W. Hagen, J.P. Hoogenboom, Fabrication of narrow-gap nanostructures using electron-beam induced deposition etch masks, *Microelectron. Eng.* 153 (2016) 77–82, <https://doi.org/10.1016/j.mee.2016.01.031>.
- [4] J.D. Wnuk, S.G. Rosenberg, J.M. Gorham, W.F. Van Dorp, C.W. Hagen, D.H. Fairbrother, Electron beam deposition for nanofabrication: insights from surface science, *Surf. Sci.* 605 (2011) 257–266, <https://doi.org/10.1016/j.susc.2010.10.035>.
- [5] J.J.L. Mulders, Purity and resistivity improvements for electron-beam-induced deposition of Pt, *Appl. Phys. A Mater. Sci. Process.* 117 (2014) 1697–1704, <https://doi.org/10.1007/s00339-014-8662-2>.
- [6] T. Aaltonen, M. Ritala, T. Sajavaara, J. Keinonen, M. Leskelä, Atomic layer deposition of platinum thin films, *Chem. Mater.* 15 (2003) 1924–1928, <https://doi.org/10.1021/cm021333t>.
- [7] A.J.M. Mackus, N.F.W. Thissen, J.J.L. Mulders, P.H.F. Trompenaars, M.A. Verheijen, A.A. Bol, W.M.M. Kessels, Direct-write atomic layer deposition of high-quality Pt nanostructures: selective growth conditions and seed layer requirements, *J. Phys. Chem. C* 117 (2013) 10788–10798, <https://doi.org/10.1021/jp402260j>.
- [8] A.J.M. Mackus, S.A.F. Dielissen, J.J.L. Mulders, W.M.M. Kessels, Nanopatterning by direct-write atomic layer deposition, *Nanoscale.* 4 (2012) 4477–4480, <https://doi.org/10.1039/c2nr30664f>.
- [9] G. Di Prima, R. Sachser, P. Gruszka, M. Hanefeld, T. Halbritter, A. Heckel, M. Huth, In situ conductance monitoring of Pt thin film growth by area-selective atomic layer deposition, *Nano Futur.* 1 (2017), <https://doi.org/10.1088/2399-1984/aa8cbb>.
- [10] M. Holz, C. Reuter, A. Ahmad, A. Reum, M. Hofmann, T. Ivanov, I.W. Rangelow, Correlative microscopy and nanofabrication with AFM integrated with SEM, *Microsc. Today* 27 (2019) 24–30, <https://doi.org/10.1017/S1551929519001068>.
- [11] C. Elbadawi, M. Toth, C.J. Lobo, Pure platinum nanostructures grown by electron beam induced deposition, *ACS Appl. Mater. Interfaces* 5 (2013) 9372–9376, <https://doi.org/10.1021/am403167d>.
- [12] N. Matsunami, Y. Yamamura, Y. Itikawa, N. Itoh, Y. Kazumata, S. Miyagawa, K. Morita, R. Shimizu, H. Tawara, Energy dependence of the ion-induced sputtering yields of monatomic solids, *At. Data Nucl. Data Tables* 31 (1984) 1–80, [https://doi.org/10.1016/0092-640X\(84\)90016-0](https://doi.org/10.1016/0092-640X(84)90016-0).
- [13] A.J.M. Mackus, N. Leick, L. Baker, W.M.M. Kessels, Catalytic combustion and dehydrogenation reactions during atomic layer deposition of platinum, *Chem. Mater.* 24 (2012) 1752–1761, <https://doi.org/10.1021/cm203812v>.
- [14] H.C.M. Knoop, S.E. Potts, A.A. Bol, W.M.M. Kessels, *Atomic Layer Deposition*, Second ed., Elsevier B.V., 2014, <https://doi.org/10.1016/B978-0-444-63304-0.00027-5>.